Study on temperature influence factors and electromagnetic heat coupling of in-wheel motor for micro-electric vehicle

Q. P. Chen

School of Mechatronics Engineering, East China Jiaotong University, 330013, Nanchang, China,
E-mail: qiping3846758@163.com

1. Introduction

With the energy drying up and worsening environment, the new energy vehicles have obtained more attentions, and electric vehicles have an extraordinary development in many countries of the world because of their advantages of emission-free, low noise, energy saving and high efficiency [1]. Permanent magnet brushless direct current motor (PMBLDCM) are often used to drive electric vehicles, which are regarded as the in-wheel motors of electric vehicles, especially the short distance transportation micro-electric vehicle. Because PMBLDCM possesses the merits of high power density, light weight, simple structure, small volume, high starting torque, strong overload capacity, good maneuverability and controllability, high reliability, low noise etc [2, 3]. In this paper, the in-wheel motor of micro-electric vehicle is PMBLDCM, which is installed in the wheel to improve the utilization rate of the body space and abandon the traditional clutch, gear, Transmission Bridge and other mechanical components. In-wheel motor has the advantages of reducing the vehicle weight, decreasing the mechanical losses and improving the driving sensitivity. In the micro-electric vehicle, the in-wheel motor possesses the narrow installation space, complex working condition, high power densities, no cooling fan and bad cooling environment and so on, which not only easily causes the temperature too high, but also reduces the work performance and service life of the in-wheel motor. Therefore, it is vital significance to study thermal loss mechanism and temperature influence factors of in-wheel motor, in order to meet the development requirements of micro-electric vehicle in efficiency, reliability and safety.

Owing to complex thermal model structure, difficulty of dealing with windings and determining of convection heat transfer coefficient and limitation of ventilation cooling system, thermal loss mechanism and temperature field influence factors of in-wheel motor in micro-electric vehicle are calculated and analyzed difficultly. Furthermore, it is more difficult to master the inner temperature change rules when there is thermal breakdown in the in-wheel motor. In order to accurately calculate inner thermal loss and temperature field distribution of in-wheel motor, a lot of researches have been conducted and many practical feasible methods were given. Referring to related articles, the methods of thermal analysis of motor mainly involve thermal parameters method, network topologic method, equivalent thermal network, the finite element method and the equivalent heat road method, etc [4]. Li and Yang [5] adopted the finite element method to study the static and transient static temperature field distribution of the pres-

sure level panel ultrasonic motor, where mechanical vibration and friction loss were calculated, and the influence of the high temperature was analyzed by the equivalent insulation, but it lacked the analysis of load influence on temperature field. Based on coupling physical field in generator, the mathematical model of temperature field was established, and the electromagnetic field and temperature field distribution were calculated and analyzed by the numerical method, but this method lacked the test [6]. Wang et al [7] applied the equivalent heat road method to calculate the thermal field distribution of motor, but the lack of test. All-around three-dimensional finite element model of temperature field was established in the claw motor of vehicle, the boundary condition problems of temperature field were handled effectively, All-around static and transient state temperature field under rated load were calculated, and the test results were in accord with the calculation results, but this method lacked the analysis of speed influence on temperature field [8]. The mathematical model of thermal loss was established, the temperature field distribution was calculated, the influence of the different voltages and frequencies on temperature distribution was simulated and analyzed, and the measurement results were in accord with the calculation results, but the lack of analysis of transient temperature field [9].

According to above analysis, the object of the present study is thermal loss and temperature field of in-wheel motor in micro-electric vehicle. In the light of the complex structure, complex heat exchange, high power density, high electromagnetic load and high thermal load in the in-wheel motor, some key factors are studied for simplicities calculation, saving time and improving accuracy. A finite element method is used to simulate and analyze thermal loss and temperature field influence factors in this paper. The mathematical model of temperature field is established, thermal loss is calculated, and the transient state temperature fields are studied under its nominal rated load. The influence of the load and revolving speed on the temperature rise of the in-wheel motor is calculated and discussed. Test bench of in-wheel motor is established, which is used to verify the rationality and effectiveness of simulation results.

2. Method and analysis

When thermal loss is analyzed, it is necessary to calculate the thermal loss of the motor, which is regarded as heat source of the motor. The total loss of the in-wheel motor is P_z which includes winding copper loss, iron core loss, permanent magnet eddy loss, mechanical loss and stray loss [8-9], as shown in Eq. (1):

$$P_z = P_{Cu} + P_{Fe} + P_{me} + P_m + P_s, \qquad (1)$$

here P_{Cu} is winding copper loss, P_{Fe} is iron core loss, P_{me} is permanent magnet eddy loss, P_m is mechanical loss, and P_s is stray loss.

In engineering field, mechanical loss and stray loss are generally determined by the motor structure, engineering experience and computational formula.

2.1. Winding copper loss

Losses caused by leakage magnetic field and leakage electric field are very small, which are easily neglected. According to the Joule's and Lenz's law, winding copper loss is equal to the product of the resistance and square of the winding current. The in-wheel motor adopts three phase winding in this paper, and the calculation formula is expressed in Eq. (2). When the motor is the transient thermal model, the inner temperature of the motor changes constantly, and the resistance value also changes constantly, therefore winding copper loss of the motor varies with time [10]. The resistance temperature formula is expressed in Eq. (3):

$$P_{Cu} = 3I^2 R_\tau ; \qquad (2)$$

$$R_\tau = R_0 (1 + \lambda \tau), \qquad (3)$$

where I is the current of each winding, R_τ is the resistance of each winding at τ, R_0 is the resistance of each winding at 0, λ is the temperature coefficient of the resistance.

2.2. Iron core loss

Alternating iron core loss and rotating iron core loss are produced because of the existence of the alternating magnetic field and rotating magnetic field. In order to calculate the iron core loss precisely, flux density change law of the iron core at any given time must be ascertained. Currently, a theory presented by Bertotti is wildly used in the engineering [7, 11]. Based on the different heat mechanism, iron core loss can be solved by separation and superposition, iron core loss consists of eddy current loss, magnetic hysteresis loss and additional losses, which coexist in the iron core. The machining accuracy of the yoke and tooth and the difference of the flux density are ignored, and iron core loss can be expressed as Eq. (4):

$$P_{Fe} = P_h + P_e + P_{ex}, \qquad (4)$$

where P_{Fe} is total iron core loss of unit mass, P_h is magnetic hysteresis loss of unit mass, P_e is eddy current loss of unit mass, and P_{ex} is additional loss of unit mass.

According to the harmonic analysis principle, any given point flux density wave in the in-wheel motor can be decomposed into a series of elliptic harmonic flux density vector. The revolving iron core losses can be equivalent to the losses produced by two quadrature magnetic fields, for each harmonic component. Magnetic hysteresis loss of unit mass is expressed as Eq. (5), eddy-current loss of unit mass is expressed as Eq. (6), and additional losses of unit mass is expressed as Eq. (7). Based on the finite element method to calculate the flux density vector waveform of each unit

within a cycle, the unit mass core loss of each unit was calculated, which then multiplied by the mass to obtain the core loss of this unit. The total core loss equals to the sum of the unit core loss of all parts:

$$P_h = \sum_{m=1}^{N} k_h m f \left(B_i^2 + B_j^2 \right) ; \qquad (5)$$

$$P_e = \sum_{m=1}^{N} k_e m^2 f^2 \left(B_i^2 + B_j^2 \right) ; \qquad (6)$$

$$P_{ex} = \frac{k_{ex}}{T_{ex}} \int_0^{T_{ex}} \left[\left(\frac{dB_i(t)}{dt} \right)^2 + \left(\frac{dB_j(t)}{dt} \right)^2 \right]^{\frac{3}{4}} dt, \qquad (7)$$

where k_h is hysteresis loss coefficient, f is actual core flux frequency, B_i is the long axis flux density, B_j is the short axis flux density, k_e is eddy current loss coefficient, k_{ex} is additional loss coefficient, and T_{ex} is flux density cycle.

2.3. Eddy current loss of permanent magnet

Permanent magnet possesses higher conductivity, which can induce the eddy. When the outer magnetic field changes, the eddy can produce the loss defined as eddy current loss of permanent magnet. Permanent magnet of in-wheel motor adopts Nd-Fe-B, which possesses the satisfactory magnetic flux density performances, but its temperature coefficient is high and its heat resistance is bad. The permanent magnet is easy to weaken magnetism when the temperature of permanent magnet becomes higher to a certain extent, which can reduce the overall performance of the motor. For these reasons, it has practical significance to calculate and analyze the eddy current loss of permanent magnet accurately. According to the magnetic induction law, the induced electromotive force and induced current which are in eddy shape can be generated in the permanent magnet. Eddy current loss of permanent magnet is expressed as Eq. (8):

$$P_{me} = \frac{L_a V k_{me}^2 f_{me}^2 B_{me}^2 L_b^2}{12 \rho_1 (L_a + L_b)} , \qquad (8)$$

where L_a is the axial length of permanent magnet, L_b is average width of permanent magnet, V is volume of permanent magnet, k_{me} is proportion constant of electromotive force, f_{me} is alternating frequency of magnetic field, B_{me} is the biggest flux density of permanent magnet, and ρ_1 is resistivity of permanent magnet.

2.4. Mechanical loss

Mechanical loss consists of bearing friction loss and ventilation loss. Bearing friction loss is expressed as Eq. (9), which is mainly affected by the machining accuracy, assembly quality, bearings quality, lubricating grease and other aspects [10, 11]. Ventilation loss is expressed as Eq. (10), which is mainly related to the motor structure, revolving speed, air gap, and stacked thick:

$$P_f = 1.5 \times 10^{-6} \frac{F}{d} v ; \qquad (9)$$

$$P_{air} = \pi\kappa_f \rho_{air} l\omega^3 r^4, \tag{10}$$

where P_f is the bearing friction loss, F is the bearing loads, d is the center diameter of bearing, v is the peripheral speed of bearing center, P_{air} is the ventilation loss, κ_f is ventilation friction loss coefficient, ρ_{air} is the air density, l is the cylinder length, ω is the revolving angular velocity, and r is the cylinder radius.

2.5. Stray loss

It is very difficult to calculate the stray loss of the in-wheel motor accurately, which is generally determined by the motor structure, engineering experience and computational formula [12, 13]. As the load increases, the wheel motor current increases, and the stray loss increases approximately with the square of the current. When the stator phase current is I_1, stray loss of the in-wheel motor can be approximately expressed as Eq. (11):

$$P_s = P_{sN}\left(\frac{I_1}{I_N}\right)^2, \tag{11}$$

where P_{sN} is the stray loss when the output power of the in-wheel motor is in rated power, and I_N is the rated current of the in-wheel motor.

2.6. Mathematical model of temperature field

According to energy conservation law and the basic principle of heat transfer, coefficient of thermal conductivity is constant for isotropic media [10]. The corresponding boundary conditions of the solution domain are established, which can be divided into three categories, which include the first boundary condition, the second boundary condition and the third boundary condition. In the Cartesian coordinate system, the transient temperature field of the in-wheel motor can be obtained by the heat conduction controlling differential equations, as shown in Eq. (12). Eq. (12) expresses the mathematical model of transient temperature field for in-wheel motor, which includes the heat conduction controlling differential equations and the boundary conditions choice equations:

$$\begin{cases} \dfrac{\partial}{\partial x}\left(\kappa_x \dfrac{\partial T}{\partial x}\right) + \dfrac{\partial}{\partial y}\left(\kappa_y \dfrac{\partial T}{\partial y}\right) + \\ \quad + \dfrac{\partial}{\partial z}\left(\kappa_z \dfrac{\partial T}{\partial z}\right) = \rho c \dfrac{dT}{dt} - q_s; \\ T\big|_{S_1} = T_0; \\ \kappa_n \dfrac{\partial T}{\partial n}\bigg|_{S_2} = -q_0; \\ \beta\left(T - T_{ev}\right) = -\kappa_n \dfrac{\partial T}{\partial n}\bigg|_{S_3}, \end{cases} \tag{12}$$

where T is the temperature varying with time t, κ_x, κ_y and κ_z are respectively the thermal conductivity of the material along the x, y, and z directions, and $\kappa_x = \kappa_y = \kappa_z$, q_s is the inner generated heat in per unit volume and per unit time, ρ is density of the motor material, and c is specific heat of the material. In static state temperature field, the temperature T does not vary with time t is time. S_1 is the boundary surface of the first class, T_0 is a known temperature during the static state heat conduction process which can also be regarded as the temperature during transient heat conduction process. S_2 is the boundary surface of the second class, n is the unit vector of boundary surface outer normal direction, κ_n is the thermal conductivity of boundary surface outer normal direction, and q_0 is boundary surface heat flux. S_3 is the third boundary surface that is convective heat transfer surface, T_{ev} is surrounding fluid temperature at the convective heat transfer boundary surface S_3, and β is the surface heat convection coefficient at the boundary surface.

2.7. Equivalent winding

Thermal model of the stator equivalent winding was established. The whole winding was regarded as an equivalent part, and thermal conductivity of the equivalent winding was calculated. Some presumptions were given [10, 11]: (a) the slot wire arrangement was well-distributed, and temperature difference was neglected; (b) insulating paint distribution of copper wire was well-distributed; (c) copper wire insulation and fill paint temperature change was linear; (d) winding impregnating paint was completely filled. Therefore, the stator slot insulation is expressed as Eq. (13), which was constituted of copper wire paint, varnish and slot insulation:

$$\varepsilon = \frac{\sum\limits_{i=1}^{n} \delta_i}{\sum\limits_{i=1}^{n} \dfrac{\delta_i}{\alpha_i}}, \tag{13}$$

where ε is the equivalent thermal conductivity coefficient of slot insulation, δ_i is the equivalent thickness of various insulating materials, α_i is the thermal conductivity coefficient of various insulating materials.

2.8. Convection heat transfer coefficient of air gap

The in-wheel motor of micro-electric vehicle adopted a closed construction, and there was no interchange of air between inner and outer environment. The air gap between stator and rotor was dealt with, and the revolving rotor made the air of air gap flow when the in-wheel motor was running. On the one hand, the flowing air is influenced by tangential motion of rotor. On the other hand, the flowing air is blocked by the inner circle surface of stator. Therefore, the complex coupling field was formed by fluid field and temperature field in the air gap. In order to simplify the calculation, the thermal conductivity coefficient of static fluid was used to describe the heat transfer ability of the flowing air in the air gap, which brought to an effective heat exchange coefficient [12, 13]. If stator inner surface and rotor outer surface are smooth, the Renault coefficient in the air gap is expressed as Eq. (14), and the Critical Renault coefficient is expressed as Eq. (15):

$$Re = \frac{\pi n \delta_{air} d_{out}}{60\tau}; \tag{14}$$

$$Re_{cr} = 41.2\sqrt{\frac{d_{in}}{\delta_{air}}} \,, \tag{15}$$

where n is the revolving speed of motor, δ_{air} is the length of air gap, d_{out} is the outer diameter of rotor, τ is the air motion viscosity coefficient, and d_{in} is the inner diameter of stator.

When $Re < Re_{cr}$, the flowing air in the air gap is laminar flow, and convection heat transfer coefficient of air gap is expressed as Eq. (16). When $Re > Re_{cr}$, the flowing air in the air gap is turbulent flow, and convection heat transfer coefficient of air gap is expressed as Eq. (17):

$$\alpha_{eff} = Nu\frac{\alpha_{air}}{d_{out}} \,; \tag{16}$$

$$\alpha_{eff} = 0.0019\left(\frac{d_{out}}{d_{in}}\right)^{-2.9084} Re^{0.4614 ln 3.33361\frac{d_{out}}{d_{in}}} \,. \tag{17}$$

Here, the convection heat transfer coefficient of air gap (α_{eff}) is 33 W/(m^2℃), the thermal conductivity of air (α_{air}) is 0.026 W/(m℃) and the anger XieErTe number (Nu) is tow.

3. Results and discussion

3.1. Establishment of finite element model

The united simulation model of in-wheel motor was established by Ansoft Maxwell and Ansys Workbench software, and thermal loss and temperature field were simulated and analyzed. According to the control requirements of micro-electric vehicle system, the main technical parameters of motor were optimized and designed by Genetic Algorithm. The structure of poles was tile shape and radial magnetization. The main technical parameters of motor were shown in Table 1. Through the symmetric simplified treatment, the three-dimensional finite element model was established, as shown in Fig. 1.

Table 1

Main technical parameters

Parameters	Value	Parameters	Value
Rated voltage	48 V	Rated power	350 W
Rated speed	1500 r/min	Phase	3
Pole number	4	Air gap	0.5 mm
Stator outer diameter	102 mm	Stator inner diameter	58.5 mm
Rotor outer diameter	57.5 mm	Rotor inner diameter	30 mm

To ensure the correctness of the magnetic circuit calculation and magnetic field analysis, the finite element meshes were manually divided by the inside selection and surface approximation method, and the solution magnetic field was divided into 197588 units. The overall mesh subdivision model is shown in Fig. 2. Fig. 2 shows that the subdivision of finite element grid is relatively uniform distribution on the whole，and the grid subdivision has a higher density in the field where the magnetic field is rela-

tively strong and changes greatly，such as the air gap part. Therefore, the subdivision of finite element grid can reach the desired effect and satisfy the accuracy of finite element calculation.
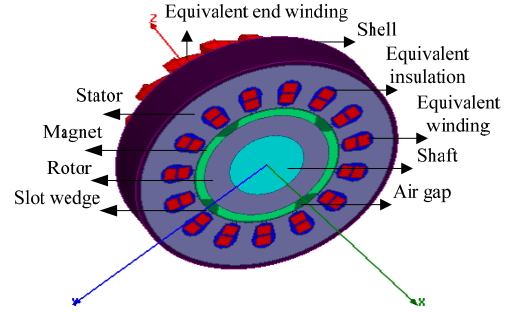
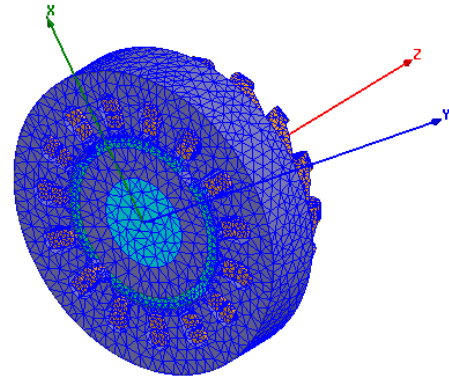

Fig. 1 Three-dimensional finite element model

Fig. 2 Overall mesh subdivision model

3.2. Analysis of thermal loss

To reduce core loss, the stator and rotor adopted the core material parameters of Toyota Prius, which was non-linear B-H characteristic. To accurately obtain the core loss, loss curves of materials with different frequency was calculated, as shown in Fig. 3. Fig. 3 shows that iron loss factor can be easily worked out. The hysteresis loss factor k_h is 184.234, the eddy loss factor k_e is 0.27, and the additional loss factor k_{ex} is 0.386.
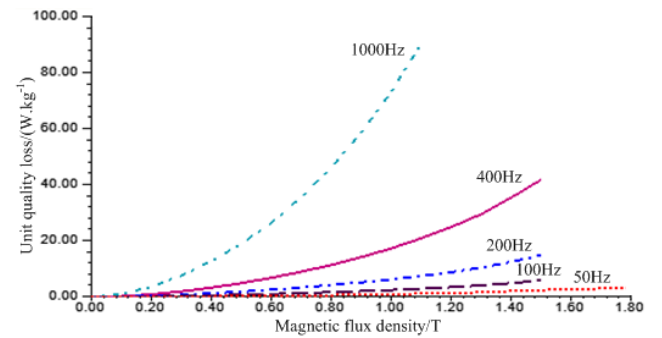

Fig. 3 Loss curves of materials with different frequency

The winding copper loss, core loss and eddy current loss of permanent magnet were calculated by Ansoft Maxwell software. The heat source loss curve is shown in Fig. 4. Fig. 4 shows that the fluctuation of winding copper loss is very large before the in-wheel motor operates at 26 ms, and the maximum amplitude is 110 W, but the fluctuations of the core loss and the eddy current loss of permanent magnet are low. As the in-wheel motor can gener-

ated a big fluctuant starting current. After the in-wheel motor operates at 26 ms, it is in stable operation, and the heat source loss tends to cyclical stability. The core loss of stator and rotor is greater than the eddy current loss of permanent magnet, but less than the winding copper loss, and the winding copper loss accounts for the main loss. In addition, Fig. 4 also shows that the winding copper loss is stability in 33 W, the core loss is stability in 3.4 W, and the eddy current loss of permanent magnet is stability in 1.6 W. According to the previous formula, it can be calculated that the mechanical loss is about 1.8 W and stray loss is about 1.5 W. The efficiency of in-wheel motor is up to 88.2%, which can fully meet the normal operation requirements of the micro-electric vehicle.
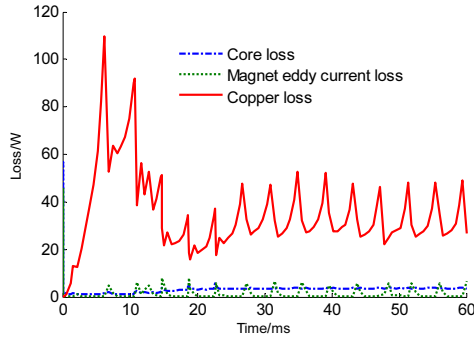

Fig. 4 Heat source loss curve

3.3. Analysis of transient temperature field

Firstly, the thermal loss was calculated by Ansoft Maxwell software, which was changed into the heat flux by Ansys Workbench software. Secondly, the heat flux was loaded in the temperature model to calculate the rise of temperature. Finally, the temperature distribution of the heat source loss and each part of in-wheel motor was obtained. When the in-wheel motor is running, all heats come from its loss. The stator and rotor, equivalent winding and permanent magnet are not only the heat source components, but also the heat transfer components, while other parts just are the heat transfer components.

When the in-wheel motor was running at the rated load, the transient state temperature field distribution was calculated, and transient temperature curve of various components was simulated, as shown in Fig. 5.
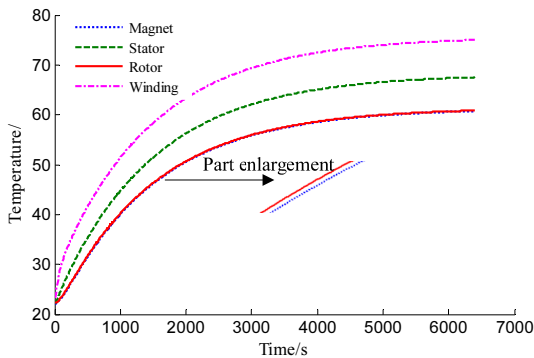

Fig. 5 Transient temperature curve of various components

Fig. 5 shows that, in the entire operation, the temperature of equivalent winding is always higher than stator temperature, and the temperature of stator is always higher than the temperature of rotor and permanent magnets. The major reasons are given: on the one hand, the copper loss

of equivalent winding is located in the stator; on the other hand, stator iron core loss is more than rotor iron core loss and the eddy current loss of permanent magnet. Temperature of the rotor and the permanent magnet is basically the same change trend and value. The major reasons are that the rotor iron core loss and the eddy current loss of permanent magnet are relatively small and the cooling environment is bad. Before 1800 s the winding temperature approximately increases linearly, temperature rising trend slows between 1800 and 4000 s, after 4000 s the temperature tends towards basic stability; Before 1650 s the stator temperature approximately increases linearly, temperature rising trend slows between 1650 and 3800 s, after 3800 s the temperature tends towards basic stability; Before 1500 s the temperature of the rotor and the permanent magnet approximately increases linearly, temperature rising trend slows between 1500 and 3600 s, after 3600 s the temperature tends towards basic stability.

3.4. Analysis of temperature influence factors

When the in-wheel motor was running stably for 1.5 hours at the rated speed of 1300 r min^{-1}, the influence of load on temperature rise is simulated, as shown in Fig. 6. Fig. 6 shows when the load of in-wheel motor is less than the rated load, the temperature rise rate of the winding and stator increases slowly. However, the load of in-wheel motor is more than 85 kg, the temperature rise rate of the winding and stator increases rapidly. At this time, the output power of the in-wheel motor increases, power loss also increases, which brings to lower efficiency.
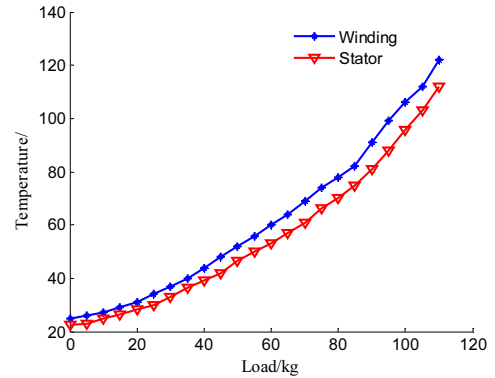

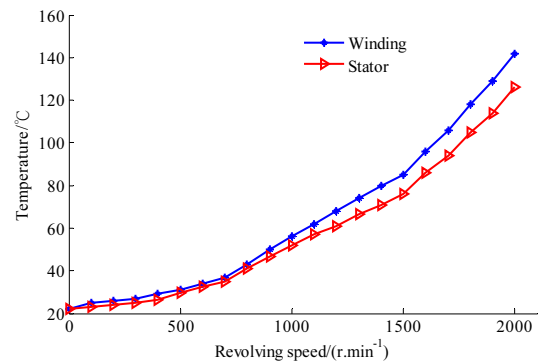Fig. 6 Influence of load on temperature rise

Fig. 7 Influence of revolving speed on temperature rise

When the in-wheel motor was running stably for 1.5 hours at the rated load, the influence of revolving speed on temperature rise is simulated, as shown in Fig. 7. Fig. 7

shows the revolving speed of in-wheel motor is less than 750 r/min, and the temperature rise rate of the winding and stator increases slowly. The revolving speed of in-wheel motor is at 750 and 1500 r/min, and the temperature rise rate of the winding and stator increases linearly. However, the revolving speed of in-wheel motor is more than 1500 r/min, the temperature rise rate of the winding and stator increases rapidly. At this time, the output power of the in-wheel motor increases, power loss also increases, which brings to lower efficiency.

Fig. 6 and Fig. 7 show that the load of in-wheel motor is more than 110 kg or the revolving speed of in-wheel motor is more than 1800 r/min, and the temperature of winding and stator can be more than 100°C, which can lead to the overheating of in-wheel motor, the burning out of winding insulation layer, the failure of Hall sensor and the demagnetization of permanent magnet, and even seriously the in-wheel motor to stall. Therefore, the load and revolving speed of the in-wheel motor have an effect on the temperature rise of in-wheel motor, while over a certain value, rise of temperature increases rapidly, which can seriously reduce the efficiency and life of in-wheel motor.

3.4. Analysis of test results

Temperature rise test of in-wheel motors was executed at rated load and ambient temperature was 22°C. The surface temperatures of in-wheel motor shell and stator were measured by the thermal infrared imager，and the temperatures of stator winding and air gap were measured by the thermistor embedded [13-15]. The comparison of the calculated results with the test average data is shown in Table 2.

Table 2
Comparison of the calculated results with the test average data

Components	Calculated results/°C	Test data/°C	Relative error/%
Stator	68.5	71.4	4.1
Stator winding	74.9	77.8	3.7
Slot wedge	69.2	71.6	3.4
Permanent magnet	62.1	65.1	4.6
Rotor	62.0	64.7	4.2
Shell	67.6	69.4	2.6

Table 2 shows that the calculated results have a slightly smaller than the test average data and the maximal relative error which can satisfy the project requirements is within 4.6%. There are two reasons for the relative error: one is system measuring error and the other is related to boundary conditions, assumptions of finite element model, the mesh quality and equivalent treatment processes method. In addition, Table also shows that the range of temperature is small among the parts, which indicates the in-wheel motor has a good heat transfer effect. The maximum measure temperature is about 77.8°C which is inferior to the maximum working temperature 100°C of Nd-Fe-B magnet and the maximum allowable temperature 120°C of B-class insulation material as well as the limit temperature 80°C of winding. Therefore, loss of excitation of permanent magnet and insulation aging are not easy to reduce, which can meet the requirements of the normal work of the in-wheel motor at the rated conditions. In a word, the simulation and test results are basically consistent.

4. Conclusions

The results of study in summary can be classified as follows:

1. The total loss of the in-wheel motor is analyzed and calculated, in order to establish the mathematical model of heat loss. Winding copper loss, stator and rotor iron core loss and eddy current loss of permanent magnet are calculated, which are coupled to the temperature field as the heat sources.

2. Mathematical model of temperature field is established. The equivalent model of stator winding is adequately handled, convection heat transfer coefficients are calculated, and the heat distribution of in-wheel motor is analyzed.

3. The united simulation model of in-wheel motor was established by Ansoft Maxwell and Ansys Workbench software, and thermal loss and temperature field were simulated and analyzed. The fluctuation of winding copper loss is very large before the in-wheel motor operates at 26 ms, and the maximum amplitude is 110 W, and the stator winding loss is the largest loss. However the fluctuations of the core loss and the eddy current loss of permanent magnet are low.

4. Transient temperature curve of various components was simulated. The temperature of equivalent winding is always higher than stator temperature, and the temperature of stator is always higher than the temperature of rotor and permanent magnets. Temperature of the rotor and the permanent magnet is basically the same change trend and value.

5. The load and revolving speed of the in-wheel motor have an effect on the temperature rise of in-wheel motor, while over a certain value, rise of temperature increases rapidly, which can seriously reduce the efficiency and life of in-wheel motor.

6. The simulation and test results are a certain relative error, but there are basically consistent.

References

1. **Yin, C.; Shen, S.** 2008. Status and trends of HEV in domestic and international, City Utility 22(3): 23-26.
2. **Guo, K.H.** 2011. The industrialization problems of electric vehicles in China, Engineering Science 13(9): 5-8.
3. **Wang, F.; Fang, Z.D.; Zhu, X.Y.** 2011. Matching, simulation and optimization of the new power transmission device for an electric vehicle, Automotive Engineering 33(9): 805-808.
4. **Chen, Q.P.; Shu, H.Y.; Zhuang, S.; Ren, K.; Fu, J.H.** 2013. Magneto-thermal coupling analysis on the in-wheel motors of micro electric vehicles, Automotive Engineering 35(7): 593-598.
5. **Li, S.Y.; Yang, M. 2010.** Analysis of the temperature

field distribution for piezoelectric plate-type ultrasonic motor, Sensors and Actuators A: Physical 164(1): 107-115.

6. **Li, J.Q.; Ma, S.L.; Li H.M. 2008.** Analysis and calculation on stator temperature field of turbo-generators based on couple physical field, Journal of North China Electric Power University 35(5): 6-10.

7. **Wang, R.; Kamper, M.J. 2005.** Development of a thermofluid model for axial field permament-magnet machines, IEEE Transactions on Energy Conversion 20(1): 80-87.
http://dx.doi.org/10.1109/TEC.2004.837301.

8. **Bao, X.H.; Wang, R.N.; Ni, Y.Y.; et al. 2011.** Calculation of rotor three dimensional temperature fields for automobile alternator, Electric Machines & Control Application 38(1): 5-10.

9. **Ying, H.; Roderick, V.N. M.; Paul, B. T.** 2003. Computational analysis of temperature rise phenomena in electric induction motors, Applied Thermal Engineering 23(7): 779-795.
http://dx.doi.org/10.1016/S1359-4311(03)00013-9.

10. **Ge, Y.Z.; Wang, S.G. 2008.** Analysis and calculation of stator temperature field of permanent magnet brushless DC motor for electric bicycle, Micromotors Servo Technique 41(12): 5-8.

11. **Lamghari Jamal, M.I.; Fouladgar, J.; Zaim, E.H.; et al.** 2006. A magneto-thermal study of a high-speed synchronous reluctance machine, IEEE Transactions on Magnetics 42(3): 1271-1274.
http://dx.doi.org/10.1109/TMAG.2006.871956.

12. **Jin, T.C.; Li, W.L.; Li, S.F.** 2006. Numerical calculation and analysis of stator thermal field in an induction machine, Electric Machines and Control 10(5): 492-497.

13. **Ho, S.L.; Fu, W.N.** 2001. Analysis of indirect temperature rise measurements of induction machines using time stepping FEM, IEEE Transactions Energy Conversion 16(1): 55-60.
http://dx.doi.org/10.1109/60.911404.

14. **Takashi, H.; Norimichi, K.** 2009. A new technique to measure the temperature of a rotating motor shaft, Applied Thermal Engineering 29(2): 317-323.

15. **Liu, Z.S.; Hou, F.X.; Yang, L.F., et al.** 2010. Research on method of vehicle durability bench test based on road profile input, Automobile Technology 40(9): 51-54.

Q. P. Chen

TEMPERATŪROS POVEIKIO IR BESIKAUPIANČIOS ELEKTROMAGNETINĖS ŠILUMOS ANT MIKRO-ELEKTRINIO AUTOMOBILIO RATO ĮMONTUOTO VARIKLIO ĮTAKOS TYRIMAS

R e z i u m ė

Tam, kad užtikrinti mikro-elektrinio automobilio efektyvumą, patikimumą ir saugumą buvo tiriamas šilumos atidavimo mechanizmas ir temperatūros įtaka rate įmontuotam varikliui. Vidiniai kompleksiniai šilumos nuostoliai ir temperatūriniai laukai buvo nustatomi baigtinių elementų metodu. Taip pat buvo sukurtas šilumos nuostolių ir temperatūrinių laukų matematinis modelis. Rate įmontuoto variklio temperatūros perdavimo procesų imitavimui ir rezultatų apdorojimui buvo naudojama jungtinė Ansoft Maxwell ir Ansys Workbench programinė įranga. Taip pat buvo ištirta apkrovų ir sukimosi greičių įtaka temperatūros didėjimui. Lyginant eksperimentinius ir proceso imitavimo rezultatus galima teigti, kad šis metodas gali būti teorinis pagrindas optimaliam rate įmontuoto variklio projektavimui.

Q. P. Chen

STUDY ON TEMPERATURE INFLUENCE FACTORS AND ELECTROMAGNETIC HEAT COUPLING ON IN-WHEEL MOTOR FOR MICRO-ELECTRIC VEHICLE

S u m m a r y

In order to meet the development requirements of micro-electric vehicle in efficiency, reliability and safety, thermal loss mechanism and temperature influence factors of in-wheel motor are study. The finite element method is used to simulate and analyze internal complex thermal loss and temperature field. The mathematical model of thermal loss and temperature field was established. The united simulation model of in-wheel motor was established by Ansoft Maxwell and Ansys Workbench software, transient state temperature were simulated and analyzed. The influences of load and revolving speed on temperature rise were also studied. The conformity of the test results with the final simulation results indicates that this method can be used to provide a theoretical basis to make further optimal design of the new driving in-wheel motor.